Glutaredoxin regulates vascular development by reversible glutathionylation of sirtuin 1

Lars Bräutigam[a,1], Lasse Dahl Ejby Jensen[b,c], Gereon Poschmann[d], Staffan Nyström[a], Sarah Bannenberg[a], Kristian Dreij[e], Klaudia Lepka[f], Timour Prozorovski[f], Sergio J. Montano[a], Orhan Aktas[f], Per Uhlén[a], Kai Stühler[d], Yihai Cao[b,c,g], Arne Holmgren[a], and Carsten Berndt[a,f,1]

[a]Department of Medical Biochemistry and Biophysics, [b]Department of Molecular Tumor and Cell Biology, and [e]Institute of Environmental Medicine, Karolinska Institutet, 17177, Stockholm, Sweden; [c]Department of Medicine and Health Sciences, Linköping University, 58183, Linköping, Sweden; [g]Department of Cardiovascular Sciences, University of Leicester, LE3 9QP Leicester, United Kingdom; and [d]Molecular Proteomics Laboratory, Biologisch-Medizinisches Forschungszentrum, and [f]Department of Neurology, Medical Faculty, Heinrich-Heine-University Düsseldorf, 40225 Düsseldorf, Germany

Edited by Michael A. Marletta, The Scripps Research Institute, La Jolla, CA, and approved November 1, 2013 (received for review July 24, 2013)

Embryonic development depends on complex and precisely orchestrated signaling pathways including specific reduction/oxidation cascades. Oxidoreductases of the thioredoxin family are key players conveying redox signals through reversible posttranslational modifications of protein thiols. The importance of this protein family during embryogenesis has recently been exemplified for glutaredoxin 2, a vertebrate-specific glutathione–disulfide oxidoreductase with a critical role for embryonic brain development. Here, we discovered an essential function of glutaredoxin 2 during vascular development. Confocal microscopy and time-lapse studies based on two-photon microscopy revealed that morpholino-based knockdown of glutaredoxin 2 in zebrafish, a model organism to study vertebrate embryogenesis, resulted in a delayed and disordered blood vessel network. We were able to show that formation of a functional vascular system requires glutaredoxin 2-dependent reversible *S*-glutathionylation of the NAD^+-dependent protein deacetylase sirtuin 1. Using mass spectrometry, we identified a cysteine residue in the conserved catalytic region of sirtuin 1 as target for glutaredoxin 2-specific deglutathionylation. Thereby, glutaredoxin 2-mediated redox regulation controls enzymatic activity of sirtuin 1, a mechanism we found to be conserved between zebrafish and humans. These results link *S*-glutathionylation to vertebrate development and successful embryonic angiogenesis.

proteomics | cardiovascular system

Embryonic development is a complex interplay between proliferation, differentiation, and apoptosis. Many signaling pathways are involved in these cellular processes, and the requirement of stringent control is obvious. The general importance of redox regulation and signaling in almost all aspects of cellular function is increasingly recognized (1), but only a limited number of specific and reversible redox signals affecting biological processes have been identified so far. Global redox signals, e.g., changes in the cellular redox state, are often transformed into specific signals by posttranslational modifications of protein cysteinyl side chains. Protein thiols can undergo a variety of modifications, disulfide formation, *S*-glutathionylation, or *S*-nitrosylation (2). Although many proteins expose cysteines (Cys) on their surface, only a few of the available thiols are targets for redox modifications, indicating that conveyance of redox signals depends on enzyme catalyzed reactions. The required enzymes are members of the thioredoxin family of proteins. Glutaredoxins (Grxs) are oxidoreductases belonging to this protein family and key enzymes controlling the redox status of protein thiols (3). This protein group can be subdivided into dithiol Grxs with a Cys-X-X-Cys active site motive and monothiol Grxs with a Cys-X-X-Ser active site motif. The catalytic activity of the latter is still elusive. Dithiol Grxs reduce disulfides via the dithiol mechanism using both cysteines of the active site motif. In addition, via the monothiol mechanism, dithiol Grxs can reduce protein–glutathione mixed disulfides (deglutathionylation) for which they require solely the *N*-terminal active site cysteine (4, 5). After reducing their substrates, oxidized Grx gets recycled by glutathione (GSH), which in turn is reduced through glutathione reductase with NADPH as final electron donor (4). Because Grxs are among the few known enzymes to be able to (de-) glutathionylate proteins, they are likely to be the main regulators for redox signaling through *S*-glutathionylation (6, 7).

Two conserved additional cysteine residues characterize Grx2 as a vertebrate-specific enzyme (8, 9). Human Grx2 is expressed in three different isoforms located in mitochondria (Grx2a) and cytosol/nucleus (Grx2b and Grx2c) (10). Zebrafish Grx2 is the closest homolog of hGrx2c and seems to be mainly localized in the cytosol (9). Recently, we showed that Grx2 is indispensable for embryonic brain development (9). In zebrafish and human cells we demonstrated that Grx2 is crucial for neuronal survival and the formation of the axonal scaffold during embryonic development of the brain via reduction of a disulfide formed within collapsin response mediator protein 2 (CRMP2), the effector protein of semaphorin 3A (Sema3A) signaling. Because many signaling systems wiring brain and vasculature are closely related (11), and the importance of Grxs and redox signaling for maintenance of cardiovascular function has previously been demonstrated (12, 13), we sought to analyze the role of Grx2 for vascular development.

Here, we describe an essential function of Grx2 for vascular development. The presented data based on a combination of biochemical and imaging tools as well as zebrafish as an accepted

Significance

Embryonic development is one of the most amazing miracles in nature. The proteins and signaling events driving this highly complex process are far from being elucidated completely. For a long time, an important role of protein reduction and oxidation during development has been assumed. Here, we demonstrate the essential role of such a regulation during cardiovascular development: The modification of a single cysteine in the protein sirtuin 1 by the vertebrate-specific oxidoreductase glutaredoxin 2 is required for vessel formation and guidance. Our data indicate that this redox-signaling pathway based on glutaredoxin-dependent reversible *S*-glutathionylation may be also important for diseases of the cardiovascular system and pathological situations connected to angiogenesis, e.g., malignancies.

Author contributions: L.B., L.D.E.J., G.P., O.A., P.U., K.S., Y.C., A.H., and C.B. designed research; L.B., L.D.E.J., G.P., S.N., S.B., K.D., K.L., T.P., K.S., and C.B. performed research; S.J.M. contributed new reagents/analytic tools; L.B., Y.C., A.H., and C.B. analyzed data; and L.B., L.D.E.J., O.A., A.H., and C.B. wrote the paper.

The authors declare no conflict of interest.

This article is a PNAS Direct Submission.

[1]To whom correspondence may be addressed. E-mail: lars.braeutigam@ki.se or Carsten.Berndt@ki.se.

This article contains supporting information online at www.pnas.org/lookup/suppl/doi:10.1073/pnas.1313753110/-/DCSupplemental.

model organism suggest that successful embryonic angiogenesis depends on the redox modification of a single-cysteine residue.

Results

ZfGrx2 was effectively knocked down to ~25% without compromising gross morphology of the embryos (Fig. S1 *A* and *B*) using a specific morpholino characterized previously (9). In fli:EGFP transgenic embryos that possess a fluorescently labeled vascular system (14), we observed a severe delay for intersegmental vessels (ISVs) to stretch beyond the midline at 35 hpf and ectopic bifurcations of ISVs at later stages upon loss of zfGrx2 (Fig. 1*A*). These findings were confirmed by two-photon time-lapse microscopy (Movie S1). Time-lapse microscopy as well as acridine orange staining (Fig. S1*C*) revealed that the observed defects are not based on increased cell death. At 48 h postfertilization (hpf), the nascent ISVs of knockdown embryos failed to establish the stereotypic vascular network. Vessels grew without regard to somitic boundaries; they formed random connections with neighboring vessels, loops, or blind ending sprouts (Fig. 1*A*). Out of 161 analyzed knockdown embryos, 83 ± 5% (mean ± SEM) showed a disordered network, in contrast to none of the controls ($n = 175$). Rescue with zfGrx2 mRNA reduced the percentage of embryos with malformations to 37 ± 8% ($n = 139$) (Fig. 1*B*). As we have previously shown that knockdown of zfGrx2 does not induce enhanced oxidative stress, we suspected a specific redox-signaling system to be disrupted by the loss of this oxidoreductase (9). To decipher the underlying molecular mechanisms, we performed rescue experiments using mutated forms of zfGrx2 with each variant having one active site cysteine exchanged to serine. This resulted in the enzymatically inactive zfGrx2C37S variant and the zfGrx2C40S mutant which is solely able to catalyze (de-) glutathionylation of thiols (4, 5). We found that only zfGrx2C40S (and not zfGrx2C37S) is able to significantly rescue vascular defects (Fig. 1*B*). The phenotype penetrance was only 33 ± 4% of 114 embryos injected with zfGrx2C40S, whereas zfGrx2C37S rescue had no effect on penetrance of the zfGrx2 knockdown phenotype (87 ± 6%, $n = 34$). These results indicated that zfGrx2 controls development of the vasculature through reversible (de-) glutathionylation. A target candidate that is regulated by glutathionylation and essential for cardiovascular development in zebrafish and mammalian systems is the NAD^+-dependent protein–deacetylase sirtuin1 (SIRT1) (15, 16). Interestingly, knockdown of SIRT1 in zebrafish phenocopies the vascular defects induced by the loss of zfGrx2 (16). In line, coinjection of zfSIRT1 together with the anti-zfGrx2 morpholino reduced the phenotypic penetrance of ISV malformation to 51 ± 9% ($n = 70$) compared with 82 ± 8% injected with the morpholino alone ($n = 117$) (Fig. 1*C* and Fig. S2). This limited, yet significant, reduction of the phenotypic penetrance is due to the observation that injection of higher amounts of zfSIRT1 mRNA was lethal in more than 50% of injected embryos. As neither *Sirt1* transcript levels (Fig. 1*D*) nor zfSIRT1 protein levels (105 ± 5% compared with WT embryos) were decreased upon loss of zfGrx2, we tested if zfGrx2 patterns the vasculature through regulation of SIRT1 enzymatic activity. Indeed, the enzymatic activity of histone–deacetylases (HDACs) was reduced to 28 ± 4% in embryos lacking zfGrx2 compared with controls (Fig. 2*A*). Rescue experiments using zfGrx2 and zfSIRT1 mRNA restored the HDAC activity to 76 ± 3% and 98 ± 2% of WT levels, respectively. Comparing HDAC activity in protein extracts of HeLa cells overexpressing hGrx2c and controls, as well as control HeLa cell extract incubated with 50 μM recombinant hGrx2c, demonstrated conservation of redox-regulated SIRT1 activation in mammals (Fig. 2*B*). Compared with control HeLa cells, SIRT1 activity increased about 2.5-fold in hGrx2c overexpressing cells (245 ± 42%) and after incubation with recombinant hGrx2c (262 ± 65%). Next, enzymatic activity was linked to *S*-glutathionylation of zfSIRT1 and specific deglutathionylation by zfGrx2. Consistent with the reported attenuation of enzymatic activity of glutathionylated human SIRT1 (15), we measured a decrease of enzymatic activity to 17 ± 4% of glutathionylated zfSIRT1 compared with fully reduced zfSIRT1 (Fig. 2*C*) in vitro. Incubation of glutathionylated zfSIRT1 with 5× molar excess of zfGrx2 restored enzymatic activity to 63 ± 8% compared with the fully reduced protein (Fig. 2*C*). Incubation of glutathionylated recombinant zfSIRT1 with zfGrx2 (single turnover: prereduced zfGrx2 in concentrations similar to zfSIRT1, catalytic conditions: 1/100 molar concentration of zfGrx2 in presence of recycling GSH) removed nearly all GSH molecules from zfSIRT1 (Fig. 3*A*). Treatment of glutathionylated zfSIRT1 with zfGrx2 (2.5× molar excess, or 1/100 molar concentration) for different periods of time confirmed time-dependent enzymatic deglutathionylation (Fig. 3*B* and Fig. S3). Amount of GSH bound to zfSIRT1 was reduced to 28.5 ± 2.1%, 22.9 ± 0.6%, and 13.0 ±

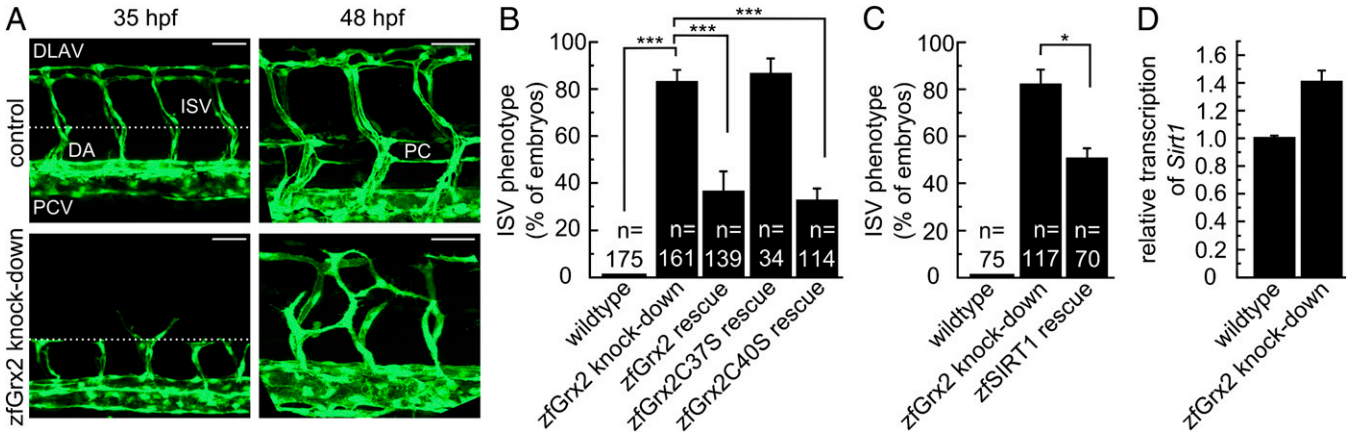

Fig. 1. zfGrx2 is essential for development of the vasculature. (*A*) Confocal microscopy of fli:EGFP transgenic embryos with or without zfGrx2 at 35 and 48 h postfertilization (hpf). DA, dorsal aorta; DLAV, dorsal longitudinal anastomotic vessel; ISV, intersegmental vessel; PC, parachordal sprouts. (Scale bars, 100 μm.) (*B*) Statistical analysis of *A* shows mean ± SEM, significance (***$P < 0.01$) was calculated by two-tailed Student's *t* test, 50 pg WT or mutated zfGrx2 mRNA were injected per single egg for rescue experiments. (*C*) Statistical analysis of intersegmental vessel formation in fli:EGFP embryos, zfGrx2 knockdown embryos, and zfGrx2 knockdown embryos rescued with 15 ng/embryo zfSIRT1 mRNA (48 hpf) (Fig. S2), mean ± SEM, significance (*$P < 0.05$) was calculated by two-tailed Student's *t* test. (*D*) Quantitative real-time PCR of zf*Sirt1* transcripts in WT and zfGrx2 knockdown embryos 48 hpf. Presented are mean ± SEM of triplicates of two independent experiments.

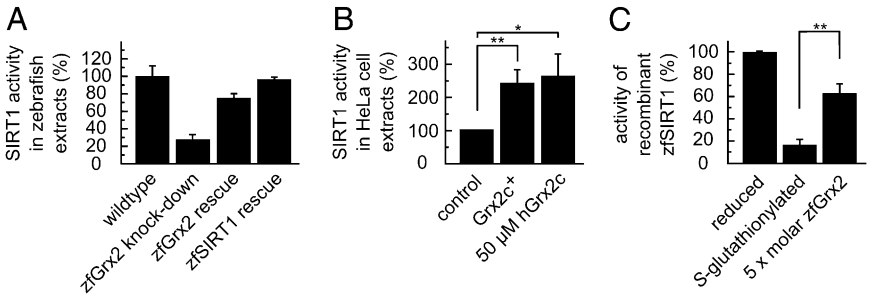

Fig. 2. Grx2 regulates enzymatic activity of SIRT1. SIRT1 activity (total histone deacetylase activity) was measured in 40 μg protein extracts obtained from WT embryos, zfGrx2 knockdown embryos, and embryos rescued with either zfGrx2 or zfSIRT1 48 hpf (*A*, mean ± SEM, duplicate measurements of two independent experiments with pooled extracts of ~200 embryos per experiment per condition) or 50 μg protein extracts of control HeLa cells, hGrx2c overexpressing HeLa cells ($Grx2c^+$), and control extract incubated with 50 μM recombinant hGrx2c (mean ± SEM, $n = 3$) (*B*). (*C*) Relative enzymatic activity of 10 μg recombinant zfSIRT1 after *S*-glutathionylation and following 30 min of incubation with 5× molar excess of prereduced zfGrx2 in relation to zfSIRT1 (mean ± SEM, $n = 3$). Significance (*$P < 0.05$, **$P < 0.01$) was calculated by two-tailed Student's *t* test.

0.5% after 0.5, 1, and 5 min, respectively. In line with results obtained in rescue experiments, zfGrx2C40S but not zfGrx2C37S was able to deglutathionylate zfSIRT1 (Fig. 3*C*). ZfGrx2C40S decreased amount of glutathionylated zfSIRT1 (100%) nearly as effective as the WT enzyme (46 ± 10% and 44 ± 6%, respectively), whereas zfGrx2C37S did not affect the glutathionylation state (98 ± 9%). Mass spectrometry identified four cysteines as target for glutathionylation in vitro, cysteines 204, 497, 681, and 765 (Figs. S4 and S5). Quantification of deglutathionylation using N-ethyl-maleimide (NEM) and its isotope labeled derivative NEMD5 revealed only cysteine 204 as substrate for zfGrx2-mediated deglutathionylation (Fig. 4*A*). Whereas no *S*-glutathionylation of this cysteine was found in the reduced protein, the intensity signal of the corresponding glutathionylated peptide was 53 ± 12% of the total signal for this peptide after treatment with glutathione disulfide (GSSG) (Fig. S6). Incubation with zfGrx2 reduced this amount to 9 ± 4%, 17 ± 7% compared with glutathionylated protein (Fig. 4*B*). In line with its regulatory effect on enzymatic activity, the identified cysteine is located in the conserved, catalytic domain of SIRT1 (Fig. S5). To confirm that glutathionylation of cysteine 204 affects enzymatic activity and is deglutathionylated specifically by Grx2, we expressed and purified a mutated form of zfSIRT1 in which cysteine 204 is exchanged to a serine residue. Indeed, activity of zfSIRT1C204S was significantly less affected after incubation with GSSG as the WT protein (Fig. 4*C*). Whereas activity of zfSIRT1 was decreased to 17 ± 7%, incubation with GSSG reduced activity of zfSIRT1C204S to only 76 ± 12%. Corroboratively, we found this variant to be less prone to *S*-glutathionylation (44 ± 5.3% compared with WT zfSIRT1) (Fig. 4*D*). Incubation of both zfSIRT1 proteins with zfGrx2 reduced the amount of *S*-glutathionylated proteins to 38 and 37% (Fig. 4*D*), further suggesting that cysteine 204 is the only specific target for deglutathionylation by zfGrx2. Mass spectrometry as well as Western blot analyses indicated that this modification appears in vivo. Compared with WT embryos, the ratio of *S*-glutathionylated versus reduced zfSIRT1 peptide signal (Fig. 4) changed from 1.2 ± 0.1 to 4.3 ± 0.4 (Fig. 5*A*), and the amount of Grx2-dependent glutathionylated zfSIRT1 increased to 354 ± 92% in zfGrx2 knockdown embryos 48 hpf (Fig. 5*B*).

Discussion

With this study, we demonstrated that zfGrx2 is critically involved in zebrafish vascular development via specific modulation of SIRT1 activity. Because we found the same regulatory interplay in a human cell system, we provide evidence that the essential role of Grx2 during vascular development might be conserved among vertebrates. In general, vascular development is highly conserved between fish and mammals, making zebrafish an accepted and suitable model for vertebrate angiogenesis (17, 18).

SIRT1 is a NAD^+-dependent protein deacetylase which is involved in a variety of metabolic processes and cellular functions including embryonic development (19). It has been shown that SIRT1 regulates neovascularization and developmental angiogenesis via FoxO and Notch signaling (16, 20). Activity of SIRT1 can be regulated via posttranslational modifications. Phosphorylation by casein kinase 2 (21–23) cyclinB/cyclin-dependent kinase 1 complex (24), or cyclin AMP-induced protein kinase A (25), methylation (26), SUMOylation (27), carbonylation (28), *S*-nitrosylation (29), and *S*-glutathionylation (15) were described as positive or negative regulatory events. Because of the last three modifications, SIRT1 is highly susceptible for redox modifications and signaling. Indeed, it has previously been shown that the role of SIRT1 in regulation of cell fate decision and its up-regulated expression after hydrogen peroxide treatment depends on GSH (30, 31).

Here, we link Grx2-dependent *S*-glutathionylation of SIRT1 to a specific developmental process (Fig. 5*C*). SIRT1 has in total 17

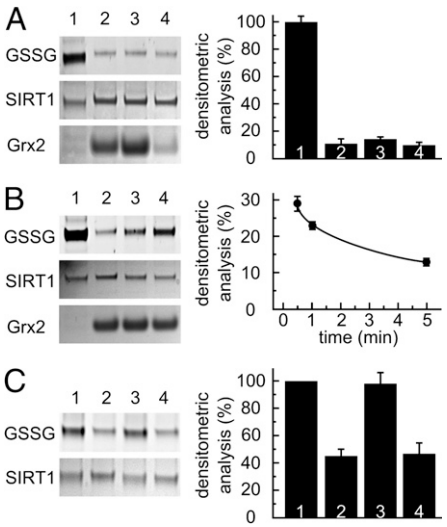

Fig. 3. zfGrx2 regulates reversible *S*-glutathionylation of zfSIRT1. (*A*) Ten micromolars zfSIRT1, *S*-glutathionylated with 0.5 mM fluorescent Eosin-Di-GSSG (1) was incubated for 10 min with prereduced zfGrx2 in single turnover conditions [50 (2) and 100 μM (3)] or in catalytic conditions [0.1 μM zfGrx2/1 mM GSH (4)] and applied to a SDS/PAGE. Bars represent the densitometric analyses for GSH bound to zfSIRT1 of two independent experiments, mean ± SEM. (*B*) Ten micromolars *S*-glutathionylated zfSIRT1was incubated without (1) or with prereduced zfGrx2 (2.5× molar excess) for 5 (2), 1 (3), and 0.5 (4) min. Samples were separated by SDS/PAGE, and relative intensity was determined after densitometric analyses for GSH bound to zfSIRT1 of two independent experiments were plotted against incubation time, mean ± SEM. (*C*) Ten micromolars S-glutathionylated zfSIRT1 (1) was incubated for 10 min with 0.1 μM zfGrx2 (2), zfGrx2C37S (3), or zfGrx2C40S (4). Bars represent the densitometric analyses for GSH bound to zfSIRT1 of two independent experiments, mean ± SEM. GSSG, fluorescence of SIRT1 after incubation with Di-Eosin-GSSG; SIRT1/Grx2, Coomassie staining of the respective proteins.

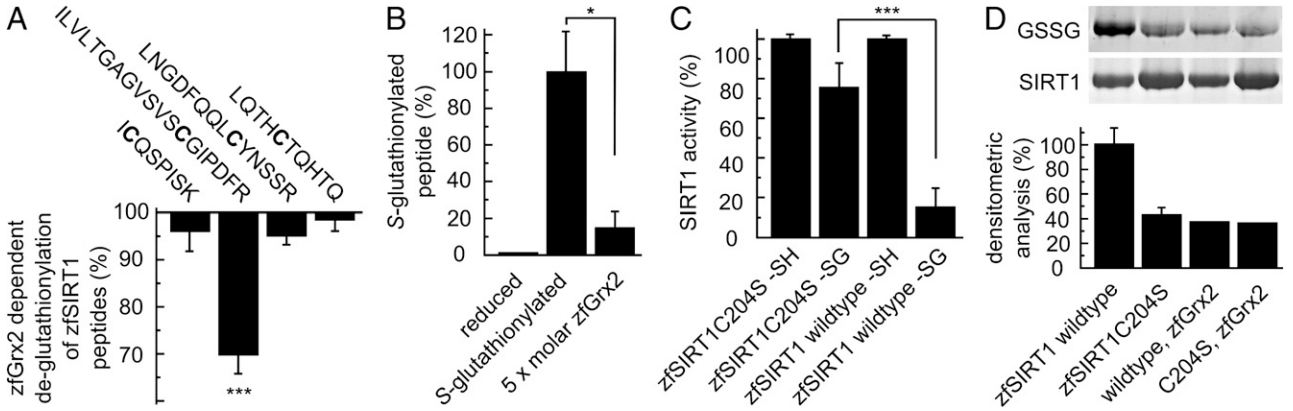

Fig. 4. One specific cysteine residue of zfSIRT1 is target for zfGrx2-dependent deglutathionylation. (*A*) Quantification of zfGrx2-dependent deglutathionylation of the four identified *S*-glutathionylated zfSIRT1 peptides by mass spectrometry using NEM and its derivative NEMD5 (mean ± SEM, $n = 6$). (*B*) Direct quantification of glutathionylated peptide of recombinant zfSIRT1 in reduced and *S*-glutathionylated protein before and after incubation with 5× molar excess of zfGrx2 for 15 min. (*C*) Activity measurements of reduced (-SH) and *S*-glutathionylated (-SG) zfSIRT and zfSIRT1C204S (mean ± SEM, $n = 3$). (*D*) Ten micromolars zfSIRT1 and zfSIRT1C204S, both *S*-glutathionylated with 0.5 mM fluorescent Eosin-Di-GSSG, with and without following incubation with prereduced zfGrx2 (2.5× molar excess) were separated by SDS/PAGE. Bars represent the densitometric analyses of GSH bound to zfSIRT1, mean ± SEM ($n = 2$). GSSG, fluorescence of SIRT1 after incubation with Di-Eosin-GSSG; SIRT1, Coomassie staining of WT and C204S proteins. Significance (*$P < 0.05$, ***$P < 0.001$) was calculated by two-tailed Student's *t* test.

cysteines, and 5 of those have been reported to be a substrate for glutathionylation in vitro using *S* nitrosoglutathione as glutathionylating agent (15). Our results clearly demonstrated that only one cysteine, Cys204 in the catalytic region, is a substrate for Grx2-mediated deglutathionylation (Fig. 4*A*). This cysteine is conserved in vertebrates and has been shown to be glutathionylated in SIRT1 in vitro (Fig. S5) (15). Two independent methods demonstrated that in embryos lacking zfGrx2 this specific cysteine is up to 3.6 times more often glutathionylated than in WT embryos (Fig. 5 *A* and *B*). We correlated the glutathionylation level of SIRT1 to its enzymatic activity (decrease of glutathionylation of about 44% is accompanied by an increase in activity of about 46%), with the modified peptide being enzymatically modulated as it has been observed before (15). The crystal structure of a SIRT1 homolog from *Archeoglobus fulgidus* revealed that the identified cysteine is in close proximity to one of the binding sites of the essential cofactor NAD^+ (32), suggesting that *S*-glutathionylation of SIRT1 might interfere with NAD^+ binding or utilization of this cofactor during the catalytic process and thereby regulates enzymatic activity.

S-glutathionylation of proteins was initially believed to be exclusively a protective mechanism against cysteine overoxidation during oxidative stress, but it is now regarded as a pivotal system for cellular signal transduction (33, 34). Both *S*-glutathionylation and Grxs have been implicated in several aspects of cardiovascular diseases (13, 33). In a mouse model, Grx1 overexpression enhanced neovascularization in the infarcted myocardium (35). The formation of new blood vessels plays a crucial role in pathological situations including cancer, as it facilitates metastasis and aggressiveness of the tumor (36). Therefore, tumor angiogenesis is one of the most promising targets for cancer therapy (37, 38). Because GSH levels have been described as important for endothelial cell differentiation (39), and altering these levels significantly influences tumor angiogenesis (40), investigating the role of Grx2-regulated SIRT1 glutathionylation in malignant angiogenesis might reveal novel therapeutic strategies. Our study extends a previous descriptive report on Grx immunoreactivity observed in early mouse development during the onset of vasculogenesis (41). We demonstrated that redox signaling based on Grx-dependent reversible *S*-glutathionylation is not only important during pathology of the cardiovascular system but also for its development.

In summary, this work expands the role of Grxs and redox signaling during vascular development and provides clear

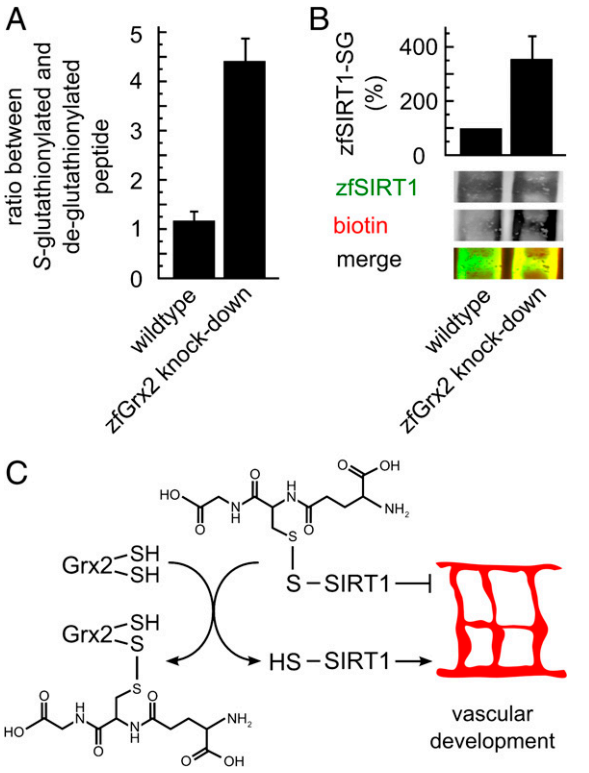

Fig. 5. Grx2 regulates vascular development via SIRT1. (*A*) Using 50 μg protein extract of zfGrx2 knockdown embryos and WT controls 48 hpf, five transitions for the glutathionylated and NEM coupled (reduced) variant of the zfSIRT1 peptide ILVLTGAGVSVSCGIPDFR were monitored using a triple quadrupole mass spectrometer, mean ± SEM ($n = 2$). (*B*) Quantification of Western Blot analyses of glutathionylated zfSIRT1 (zfSIRT1-SG) after biotin labeling of Grx2-specific deglutathionylated thiols in zebrafish embryos 48 hpf, mean ± SEM ($n = 4$). Bars represent the densitometric analyses of glutathionylated zfSIRT1/total zfSIRT1. (*C*) Grx2 is essential for vascular development via activation of SIRT1 through reversible *S*-glutathionylation of a cysteine residue located in the catalytic domain of this protein deacetylase.

evidence that *S*-glutathionylation is an essential posttranslational modification required for successful embryonic development.

Materials and Methods

Cell Culturing. HeLa cells or cells stably overexpressing hGrx2c (42) were cultivated in DMEM (1 g/L D-glucose) supplemented with 10% (vol/vol) FCS, 2 mM glutamine, and 100 U/mL penicillin/streptomycin (PAA) at 37 °C in humidified atmosphere containing 5% (vol/vol) CO_2.

Zebrafish Husbandry. Zebrafish were kept in a 10/14 h dark/light cycle under standard conditions. Embryos were obtained from natural matings, raised following established protocols (43), and staged according to Kimmel (44) in hours postfertilization (hpf). All experiments were performed in compliance with the North Stockholm Ethical council. In this study, the fli:EGFP (14) transgenic line was used.

Morpholino and mRNA Injections. The morpholino knocking down zfGrx2 was designed and obtained from Genetools (www.gene-tools.com) and described previously (9). It was dissolved to 3 mM in ddH_20, diluted with injection buffer (3 μM spermine, 0.7 mM spermidine, and 0.1% phenol red in PBS), and 1.5 nL of a 75-nM solution was injected into one single-cell embryo using a Femtojet microinjector (Eppendorf). For rescue experiments, capped mRNA of the respective constructs was synthesized with the mMessage/Machine Kit (Ambion) and injected together with the morpholino. The rescue construct did not contain the morpholino attachment site, as this is located in the direct upstream region of the translational start codon. Cloning of zfGrx2 variants for capped mRNA synthesis has been described previously (9); the EST encoding for zfSIRT1 was obtained from Source BioScience (IMAGE: 7148963) and was directly used as a template for capped mRNA synthesis.

Quantitative Real-Time PCR. Quantification of gene expression was performed in triplicates using Maxima SYBR Green qPCR Master Mix (Fermentas) with detection on an AB 7500 Real-Time PCR System (Applied Biosystems). The reaction cycles used were 95 °C for 2 min followed by 40 cycles at 95 °C for 15 s and 60 °C for 1 min followed by melt curve analysis. Relative gene expression quantification of SIRT1 was based on the comparative threshold cycle method ($2 - \Delta\Delta Ct$) using ACTB and EF1A as endogenous control genes. Primer sequences are given in Table S1. Three independent experiments were evaluated.

Western Blot. For Western blot analyses, protein extracts of ~200 zebrafish embryos were produced as described previously (9). Fifty to eighty micrograms extract were loaded on SDS/PAGE (Pierce) and transferred to nitrocellulose membrane using the iBlot system (Invitrogen). zfGrx2 and zfSIRT1 were visualized using in-house made specific primary antibodies [rabbit anti-zfGrx2 (9), chicken anti-mouse SIRT1], biotinylated antibodies (Invitrogen), and streptavidin-coupled infrared antibodies (LI-COR).

Expression and Purification of Recombinant Proteins. Zebrafish Grx2 was cloned and purified as previously described (9). ZfSIRT1 has been subcloned in pet15b using the primer pair 5′-atggcggacggcgaaaataaacg-3′/5′- ttattgtgtgtgttgtgtgc-3′. ZfSIRT1C204S has been cloned by rolling circle PCR using the primers 5′-tgtctgtttccagtgggattcc-3′ and 5′-ggaatcccactggaaacagaca-3′. The respective proteins were expressed and purified as previously described (9, 45).

HDAC Activity Measurements. The HDAC activity was determined with the Fluor de lys-Green HDAC assay kit (Enzo) using 40 μg of zebrafish protein extract, 50 μg of HeLa cell extract, or 10 μg recombinant zfSIRT1 per measurement following the manufacturer's instructions. Protein of zebrafish embryos (~200 embryos/group) has been extracted in the presence of NEM as described earlier (9). HeLa cells were extracted using radioimmunoprecipitation assay buffer including 10 mM NEM.

Determination of *S*-Glutathionylation in Vitro and in Vivo. To measure deglutathionylation of SIRT1 in vitro, the protein was prereduced [10 mM DTT and 10 mM Tris(2-carboxyethyl)phosphine hydrochloride for 30 min at RT] followed by desalting (ZebaSpin, Thermo Scientific) and incubation with 5× excess of fluorescent Di-Eosin-glutathione disulfide (46) for 1 h at 37 °C, with subsequent desalting. Glutathionylated SIRT1 was incubated with prereduced zfGrx2 (10 mM DTT, 10 mM TECP for 30 min at RT). We used 5× excess of zfGrx2 protein, because zfSIRT1 has 17 cysteine residues, of which at least 5 are surface exposed and accessible for redox regulation (15). After separation on a non-reducing SDS page, fluorescent bands were documented under UV light, and proteins were stained with Coomassie; band intensity was measured by densitometry. Three independent sets of experiments were evaluated. For mass spectrometry, 50 μM recombinant zfSIRT1 were reduced (10 mM DTT for 15 min at RT), desalted, incubated for 15 min at 37 °C with 5 mM nonfluorescent glutathione disulfide, and deglutathionylated with 5× molar excess of zfGrx2 (15 min at RT). To determine glutathionylation state of zfSIRT1 in vivo, 0.1–1 mg NEM-treated protein extract of zebrafish embryos 48 hpf were desalted (ZebaSpin, Thermo Scientific) and incubated for 1 h at RT with 10 μM zfGrx2C40S and 2 mM GSH to deglutathionylate Grx2-specific substrates. Reduced thiols were labeled with biotin–maleimide (0.02 μg/mL, Sigma) for 1 h at RT. Samples were prepared for Western blot analysis either without or following trichloroacetic acid precipitation.

Mass Spectrometry and Mass Spectrometric Data Analysis. For direct detection and quantification of glutathionylated peptides, protein samples including 5 μg zfSIRT1 were loaded on a SDS polyacrylamide gel, stained with Coomassie brilliant blue, destained, alkylated with iodoacetamide (55 mM in an aqueous solution containing 50 mM ammonium bicarbonate), and digested with trypsin. Peptides were extracted from the gel with 0.1% trifluoroacetic acid and subjected to liquid chromatography. For stable isotope-based quantification of modified cysteine residues, free thiol groups of zfSIRT1 were blocked by NEM (10 mM) and after SDS polyacrylamide gel separation reduced with DTT (10 mM in an aqueous solution containing 50 mM ammonium bicarbonate). After Coomassie staining, newly accessible thiol groups of zfSIRT1 were labeled with a five-deuterium-atoms-containing heavy version of *N*-ethyl-maleimide (NEMD5, 50 mM in 20 mM Tris pH 7) or in a control reaction with NEM (50 mM in 20 mM Tris pH 7) and digested and prepared for liquid chromatography as described above. For peptide separation over a 55-min LC gradient, an Ultimate 3000 Rapid Separation liquid chromatography system (Dionex/Thermo Scientific) equipped with an Acclaim PepMap 100 C18 column (75-μm inner diameter, 25- or 50-cm length, 2-μm particle size) from Dionex/Thermo Scientific was used. Mass spectrometry was carried out on an Obitrap Elite high-resolution instrument (Thermo Scientific) operated in positive mode and equipped with a nano electrospray ionization source. Capillary temperature was set to 275 °C, and source voltage was set to 1.5 kV. Survey scans were carried out in the orbitrap analyzer over a mass range from 350 to 1,700 *m/z* at a resolution of 60,000 (at 400 *m/z*). The target value for the automatic gain control was 1,000,000, and the maximum fill time was 200 ms. The 10 or 15 most intense doubly and triply charged peptide ions (minimal signal intensity 500) were isolated, transferred to the linear ion trap part of the instrument, and fragmented using collision-induced dissociation. Peptide fragments were analyzed using a maximal fill time of 200 ms and automatic gain control target value of 100,000. The available mass range was 200–2000 *m/z* at a resolution of 5,400 (at 400 *m/z*). Already fragmented ions were excluded from fragmentation for 45 s.

Raw files were further processed for protein and peptide identification and quantification using the MaxQuant software suite version 1.3.0.5 (Max Planck Institute of Biochemistry). Within the software suite, database searches were carried out using 40,537 *Danio rerio* sequences from the UniProt/SwissProt database (release 02.2013, proteome dataset) using the following parameters: mass tolerance Fourier transformed mass spectra (Orbitrap) first/second search: 20 ppm/6 ppm, mass tolerance fragment spectra (linear ion trap): 0.4 Da, variable modification: glutathione, carbamidomethyl, methionine oxidation, acetylation at protein *N* termini. The following variable modifications were considered for searching NEM-treated zfSIRT1 samples: methionine oxidation, acetylation at protein *N* termini, NEM, and NEMD5. Peptides, proteins, and modification assignments were accepted at a false discovery rate of 1%. Quantification of 2+, 3+, and 4+ peptide ions of modified and unmodified versions of cysteine-containing peptides was carried out by the integration of extracted ion chromatogram (10 ppm mass and 3-min time window) areas using Xcalibur 2.2 SP1.48 Qual Browser (Thermo Scientific), whereas specificity of the signals for the glutathionylated and NEMD5 labeled peptides was additionally controlled by analyzing reduced and doubly NEM labeled samples, respectively. Summed signals of the detectable charge states were used as quantitative correlate for relative peptide amounts.

For targeted quantification of zfSIRT1 peptides from one-dimensional gel bands of tryptic digested lysates of WT and Grx2 knockdown fishes, peptides were separated by online reversed-phase nanoHPLC (Ulimate 3000, Dionex/Thermo Scientific) over a 15-min gradient using an Acclaim PepMap 100 C18 column (75-μm inner diameter, 15-cm length, 2-μm particle size from Dionex/Thermo Scientific). Subsequent targeted mass spectrometric analysis was carried out using a Thermo Scientific triple stage quadrupole (TSQ) Vantage mass spectrometer (Thermo Scientific, Xcalibur 2.1.0 SP1, and TSQ Tune Master 2.3.0.1209 SP2 operation software) in positive mode. Instrument

parameters include a spray voltage of 1,400 V, 275 °C capillary temperature, a quadrupole 1 and 2 resolution of 0.7 FWHM, a Q2 Argon gas pressure of 1.5 milliTorr, and a total cycle time of 2 s. The collision energy was optimized using recombinant zfSIRT1. Following masses (in *m/z*) were monitored: Q1: 737.0378, Q3: 534.2665, 704.3721, 1112.449, 1199.481, 1298.55 (ILVLTGAGVSVSC[Glutathione]GIPDFR, 3x charged precursor); Q1: 1015.0429, Q3: 534.2665, 1019.461, 1118.529, 1205.561, 1495.818 (ILVLTGAGVSVSC[NEM]GIPDFR, 2× charged precursor); Q1: 732.8833, Q3: 457.2512, 585.3098, 845.4623, 1008.526, 1136.584 (LGASQYLFQAPNR, 2× charged precursor); Q1: 967.9945, Q3: 445.2764, 516.3135, 872.483, 1201.642, 734.3463 (NYTQNIDTLEQVAGIQK, 2× charged precursor). The specificity of monitored transitions was controlled by spiking in recombinant zfSirt1 in selected samples before one-dimensional gel separation. The triple quadrupole data were analyzed using Pinpoint 1.2.0 software (Thermo Scientific).

Microscopy, Image Processing, and Statistics. For live imaging of ISV sprouting, two-photon laser-scanning microscopy was used. Transgenic fli:EGFP embryos were embedded in low-melting (LM) agarose in a Petri dish supplemented with tricaine and 1-phenyl-2-thiourea (Sigma). The dish was mounted on a computer-controlled stage bolted to an upright two-photon laser-scanning microscope (2PLSM, Zeiss LSM510 META NLO), equipped with a 40×/1.0 water dipping lens (Zeiss) and a Ti:Sapphire tunable Chameleon Ultra-II infrared laser (Coherent). EGFP was excited with 910 nm. Laser power was kept at a minimum. Imaging was performed at 28 °C using a temperature-controlled chamber (Warner Instruments); the interval between each time-point (*z* stack) was 10 min. Movies were rendered from maximum projections of the optical slices of each time-point (*z* stack) using the ImageJ image analysis software (http://imagej.nih.gov). Laser-scanning microscopy images were taken of fixed specimen mounted in glycerol or living embryos embedded in LM agarose with a Zeiss LSM700 confocal microscope and bright-field pictures with a Leica MZ16 microscope equipped with a Leica DFC300FX camera. Images were processed with ImageJ and Gimp (www.gimp.org) without obscuring any original data.

All data were expressed as mean ± SEM. Statistical significance of datasets with $n \geq 3$ was calculated using two-tailed Student's *t* test.

ACKNOWLEDGMENTS. We thank Lena Ringdén for administrative assistance and the zebrafish facility of the Karolinska Institutet for excellent service. Lucia Coppo (Stockholm) and Eva Hawranke (Düsseldorf) contributed to experimental work. Michael Potente (Goethe-University Frankfurt am Main, Germany) is acknowledged for helpful discussions. This work was supported by Karolinska Institutet [postdoctoral fellowships (to C.B.), PhD fellowship 2379/07-225 (to L.B.)], the Heinrich Heine University research commission of the Medical Faculty (to O.A. and C.B.), PhD fellowship by Graduate School iBrain (to K.L.), CLICK imaging facility and KAW 2006.0192 (to A.H.), the Swedish Cancer Society (961) (to A.H.), and the Swedish Research Council (K2012-68X-03529-41-3) (to A.H.).

1. Ufer C, Wang CC, Borchert A, Heydeck D, Kuhn H (2010) Redox control in mammalian embryo development. *Antioxid Redox Signal* 13(6):833–875.
2. Hanschmann E-M, Godoy JR, Berndt C, Hudemann C, Lillig CH (2013) Thioredoxins, glutaredoxins, and peroxiredoxins-molecular mechanisms and health significance: From cofactors to antioxidants to redox signaling. *Antioxid Redox Signal* 19(13):1539–1605.
3. Holmgren A, et al. (2005) Thiol redox control via thioredoxin and glutaredoxin systems. *Biochem Soc Trans* 33(Pt 6):1375–1377.
4. Lillig CH, Berndt C, Holmgren A (2008) Glutaredoxin systems. *Biochimica et Biophysica Acta* 1780(11):1304–1317.
5. Lillig CH, Berndt C (2013) Glutaredoxins in thiol/disulfide exchange. *Antioxid Redox Signal* 18(13):1654–1665.
6. Gallogly MM, Starke DW, Mieyal JJ (2009) Mechanistic and kinetic details of catalysis of thiol-disulfide exchange by glutaredoxins and potential mechanisms of regulation. *Antioxid Redox Signal* 11(5):1059–1081.
7. Gallogly MM, Mieyal JJ (2007) Mechanisms of reversible protein glutathionylation in redox signaling and oxidative stress. *Curr Opin Pharmacol* 7(4):381–391.
8. Sagemark J, et al. (2007) Redox properties and evolution of human glutaredoxins. *Proteins* 68(4):879–892.
9. Bräutigam L, et al. (2011) Vertebrate-specific glutaredoxin is essential for brain development. *Proc Natl Acad Sci USA* 108(51):20532–20537.
10. Lönn ME, et al. (2008) Expression pattern of human glutaredoxin 2 isoforms: Identification and characterization of two testis/cancer cell-specific isoforms. *Antioxid Redox Signal* 10(3):547–557.
11. Adams RH, Eichmann A (2010) Axon guidance molecules in vascular patterning. *Cold Spring Harb Perspect Biol* 2(5):a001875.
12. Ushio-Fukai M (2006) Redox signaling in angiogenesis: Role of NADPH oxidase. *Cardiovasc Res* 71(2):226–235.
13. Berndt C, Lillig CH, Holmgren A (2007) Thiol-based mechanisms of the thioredoxin and glutaredoxin systems: Implications for diseases in the cardiovascular system. *Am J Physiol Heart Circ Physiol* 292(3):H1227–H1236.
14. Lawson ND, Weinstein BM (2002) In vivo imaging of embryonic vascular development using transgenic zebrafish. *Dev Biol* 248(2):307–318.
15. Zee RS, et al. (2010) Redox regulation of sirtuin-1 by S-glutathiolation. *Antioxid Redox Signal* 13(7):1023–1032.
16. Potente M, et al. (2007) SIRT1 controls endothelial angiogenic functions during vascular growth. *Genes Dev* 21(20):2644–2658.
17. Tobia C, De Sena G, Presta M (2011) Zebrafish embryo, a tool to study tumor angiogenesis. *Int J Dev Biol* 55(4-5):505–509.
18. Baldessari D, Mione M (2008) How to create the vascular tree? (Latest) help from the zebrafish. *Pharmacol Ther* 118(2):206–230.
19. Knight JRP, Milner J (2012) SIRT1, metabolism and cancer. *Curr Opin Oncol* 24(1):68–75.
20. Guarani V, et al. (2011) Acetylation-dependent regulation of endothelial Notch signalling by the SIRT1 deacetylase. *Nature* 473(7346):234–238.
21. Zschoernig B, Mahlknecht U (2009) Carboxy-terminal phosphorylation of SIRT1 by protein kinase CK2. *Biochem Biophys Res Commun* 381(3):372–377.
22. Kang H, Jung J-W, Kim MK, Chung JH (2009) CK2 is the regulator of SIRT1 substrate-binding affinity, deacetylase activity and cellular response to DNA-damage. *PLoS ONE* 4(8):e6611.
23. Dixit D, Sharma V, Ghosh S, Mehta VS, Sen E (2012) Inhibition of Casein kinase-2 induces p53-dependent cell cycle arrest and sensitizes glioblastoma cells to tumor necrosis factor (TNFα)-induced apoptosis through SIRT1 inhibition. *Cell Death Dis* 3:e271.
24. Sasaki T, et al. (2008) Phosphorylation regulates SIRT1 function. *PLoS ONE* 3(12):e4020.
25. Gerhart-Hines Z, et al. (2011) The cAMP/PKA pathway rapidly activates SIRT1 to promote fatty acid oxidation independently of changes in NAD(+). *Mol Cell* 44(6):851–863.
26. Liu X, et al. (2011) Methyltransferase Set7/9 regulates p53 activity by interacting with Sirtuin 1 (SIRT1). *Proc Natl Acad Sci USA* 108(5):1925–1930.
27. Yang Y, et al. (2007) SIRT1 sumoylation regulates its deacetylase activity and cellular response to genotoxic stress. *Nat Cell Biol* 9(11):1253–1262.
28. Caito S, et al. (2010) SIRT1 is a redox-sensitive deacetylase that is post-translationally modified by oxidants and carbonyl stress. *FASEB J* 24(9):3145–3159.
29. Kornberg MD, et al. (2010) GAPDH mediates nitrosylation of nuclear proteins. *Nat Cell Biol* 12(11):1094–1100.
30. Prozorovski T, et al. (2008) Sirt1 contributes critically to the redox-dependent fate of neural progenitors. *Nat Cell Biol* 10(4):385–394.
31. Fratelli M, et al. (2005) Gene expression profiling reveals a signaling role of glutathione in redox regulation. *Proc Natl Acad Sci USA* 102(39):13998–14003.
32. Min J, Landry J, Sternglanz R, Xu RM (2001) Crystal structure of a SIR2 homolog-NAD complex. *Cell* 105(2):269–279.
33. Mieyal JJ, Gallogly MM, Qanungo S, Sabens EA, Shelton MD (2008) Molecular mechanisms and clinical implications of reversible protein S-glutathionylation. *Antioxid Redox Signal* 10(11):1941–1988.
34. Dalle-Donne I, Rossi R, Giustarini D, Colombo R, Milzani A (2007) S-glutathionylation in protein redox regulation. *Free Radic Biol Med* 43(6):883–898.
35. Adluri RS, et al. (2012) Glutaredoxin-1 overexpression enhances neovascularization and diminishes ventricular remodeling in chronic myocardial infarction. *PLoS ONE* 7(3):e34790.
36. Chung AS, Ferrara N (2011) Developmental and pathological angiogenesis. *Annu Rev Cell Dev Biol* 27:563–584.
37. Shojaei F (2012) Anti-angiogenesis therapy in cancer: current challenges and future perspectives. *Cancer Lett* 320(2):130–137.
38. Cao Y, et al. (2011) Forty-year journey of angiogenesis translational research. *Sci Transl Med* 3(114), 10.1126/scitranslmed.3003149.
39. Mallery SR, Lantry LE, Laufman HB, Stephens RE, Brierley GP (1993) Modulation of human microvascular endothelial cell bioenergetic status and glutathione levels during proliferative and differentiated growth. *J Cell Biochem* 53(4):360–372.
40. Albini A, et al. (2001) Inhibition of angiogenesis-driven Kaposi's sarcoma tumor growth in nude mice by oral N-acetylcysteine. *Cancer Res* 61(22):8171–8178.
41. Kobayashi M, Nakamura H, Yodoi J, Shiota K (2000) Immunohistochemical localization of thioredoxin and glutaredoxin in mouse embryos and fetuses. *Antioxid Redox Signal* 2(4):653–663.
42. Enoksson M, et al. (2005) Overexpression of glutaredoxin 2 attenuates apoptosis by preventing cytochrome c release. *Biochem Biophys Res Commun* 327(3):774–779.
43. Westfield M (2000) *The Zebrafish Book. A Guide for the Laboratory Use of Zebrafish (Danio rerio)* (Univ. of Oregon Press, Eugene, OR).
44. Kimmel CB, Ballard WW, Kimmel SR, Ullmann B, Schilling TF (1995) Stages of embryonic development of the zebrafish. *Dev Dyn* 203(3):253–310.
45. Liu Y, Gerber R, Wu J, Tsuruda T, McCarter JD (2008) High-throughput assays for sirtuin enzymes: A microfluidic mobility shift assay and a bioluminescence assay. *Anal Biochem* 378(1):53–59.
46. Raturi A, Mutus B (2007) Characterization of redox state and reductase activity of protein disulfide isomerase under different redox environments using a sensitive fluorescent assay. *Free Radic Biol Med* 43(1):62–70.